Int J Fract (2010) 165:175–188
DOI 10.1007/s10704-010-9476-7

ORIGINAL PAPER

Criterion for initiation of cracks under mixed-mode I + III loading

Bisen Lin · M. E. Mear · K. Ravi-Chandar

Received: 21 July 2009 / Accepted: 4 March 2010 / Published online: 18 June 2010

Abstract The initiation of crack growth under a combination of opening and anti-plane shearing mode loading is considered in this paper. It is shown that such cracks do not grow through a continuous evolution of the crack surface. Rather, an abrupt fragmentation or segmentation of the crack front is generated. Through experimental observations and a theoretical model, we postulate a relationship between the scale of the fragmentation and the mode mix.

Keywords Fracture · Three-dimensional loading · Crack front fragmentation

1 Introduction

A long-standing unsolved problem in fracture mechanics concerns the criterion for fracture under combined loading modes I + III. Even in the simplest setting of linearly elastic fracture mechanics, formulation of the fracture criterion is incomplete. Implicit in the present formulation is the existence of a K-dominant region about the crack front such that linearly elastic fracture mechanics pertains; in the present context this not only involves the usual notion that inelastic behavior, etc. be confined to a small process zone ahead of the crack tip, but also that the crack surface be sufficiently regular that (apart from "isolated" points or edges) the singular elastic field about the crack front exhibits the standard square-root behavior. We hasten to add that this is not a limitation, but a starting point, much as in the development of LEFM for 2-D problems.

A major distinction between crack growth under mixed modes I + II and three dimensional crack growth under mixed modes I + III arises from the geometric constraint associated with the three-dimensional evolution of the fracture surface. For a three-dimensional crack under combined modes I + II, as long as the gradients along the crack front are small, it is sufficient to adopt a 2-D description in which the crack front is described by a point and the crack path by a line, and furthermore, the crack path (which may evolve smoothly or may suffer discontinuities in slope as a result of discontinuities in loading) can be determined from the criterion of local symmetry which insists that the crack will choose the path along which there is locally opening mode deformation.

In contrast, in the mixed mode I + III crack problem the crack front is a curve (perhaps tortuous and/or kinked) and the crack path is a warped surface, possibly continuous but most likely faceted or segmented with steps. Possible continuous and faceted or segmented crack growth modes under mixed mode I + III loading are illustrated in Fig. 1. It is important to recognize that

B. Lin · M. E. Mear · K. Ravi-Chandar (✉)
Center for Mechanics of Solids, Structures and Materials,
The University of Texas at Austin, Austin,
TX 78712-0235, USA
e-mail: kravi@mail.utexas.edu

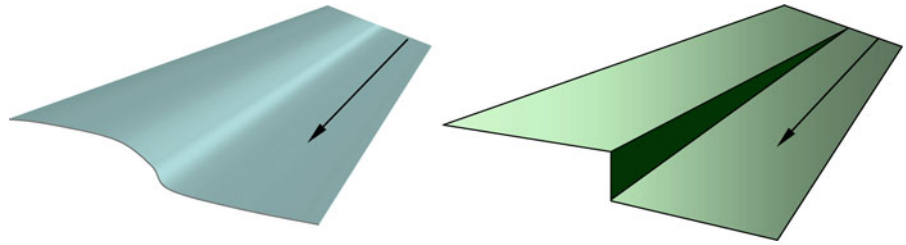

Fig. 1 Schematic illustration of continuous and segmented evolution of a fracture surface under mode I + III loading. The *arrows* indicate the direction of crack propagation

obvious generalizations of the 2-D criterion of local symmetry cannot be applied easily to mixed-mode 3-D cracks. Reasons that such a generalization should not be expected to apply include the following:

Loss of local symmetry It is in general impossible to enforce the absence of shear deformations simultaneously at all locations along the crack front and still insist upon a continuous crack surface evolution. In particular, it is not possible to satisfy a condition in which both the mode II and mode III stress intensity factors vanish along a smooth crack front. This implies that the criterion must involve a combination of at least two stress intensity factors. Of course, this limitation can be removed by allowing for the fact that the crack front may fragment into multiple cracks.

Loss of self-similarity Since more than one stress intensity factor must typically be involved in the growth criterion, the process zone ahead of a growing crack front need not maintain self-similarity. Even if (as assumed) small scale yielding conditions pertain, the "critical condition" for growth may exhibit a complicated dependence upon mode mixity. We remark that a similar situation exists for interface cracks under mixed modes I + II, for which the effective crack toughness depends strongly upon mode mix.

Non-locality While the criterion for growth in 2-D is necessarily local (involving the stress intensity factors at the crack tip), the growth criterion for 3-D is likely to be non-local in the sense that it involves the neighborhood of a point on the crack front. Although there have been recent mathematically-based proposals for the possible structure of 3-D growth laws exhibiting non-locality (see Hodogdon and Sethna 1993), this issue has not been considered in sufficient detail to be properly understood.

Loss of geometric constraint—facet/step creation There is likely to be a significant energy penalty associated with continuous crack surface evolution under mixed-mode loading, and this introduces a competition with possible faceting which, while itself introducing additional energy associated with facet creation, can lead to a reduction in overall energy by releasing the geometrical constraint (which may manifest itself as the non-locality described above). The dependence of faceting upon mode mixity, as well as upon relevant geometric (and, possibly microstructural) length scales has not yet been explored in detail.

Such fundamental differences between the nature of 3-D and 2-D crack growth illuminate the difficulties inherent in the development of growth laws for three-dimensional fracture. The purpose of the present investigation is first and foremost to provide an enhanced understanding of the complex phenomenon of three-dimensional crack growth, and this necessitates that each of the complicating features described above (and, possibly, others to be revealed by the experimental studies) be considered. Through an integrated experimental, computational and modeling effort we explore the problem of three dimensional mixed mode fracture and attempt to answer the above fundamental questions.

This paper is organized as follows: first, we discuss in Sect. 2 the few experimental and theoretical studies that have been performed in this area in order to provide a proper perspective for the study reported here. This is followed in Sect. 3 by a description of a criterion that is expected to capture crack front fragmentation. The design of the specimen, analysis of the three dimensional stress state of the specimen, and the experimental methods used to determine the mixed mode fracture conditions are discussed in Sect. 4. An interpretation of the experimental observations is used in Sect. 5 to calibrate the criterion for crack front fragmentation criterion. The major conclusions are summarized in Sect. 6.

2 Review of prior work on mixed mode I + III fracture

There are many experimental observations concerning crack growth under loading conditions that impose at least a small component of mode III loading. The early observations of fracture "lances" by Smekal (1953) were followed by Sommer (1969) who observed a transition from a continuous evolution of the crack surface to a faceted crack evolution, as shown in Fig. 2a. This was generated by superposing a small torsional loading on a bar of circular cross-section in which an opening mode crack was generated by internal pressure. Thus, under dominant mode I loading, the crack grew initially in a self similar manner in the central region; but beyond a certain radius, as the shear stress from the torque increased from the center, an abrupt transition in the fracture surface to a faceted, multi-crack evolution was observed. Through a detailed examination of the topography of the fracture surface Sommer showed that there was a critical combination of the global mode I and mode III loading at which the crack front segmented into facets that make an angle of about 3.3° with respect to the nominal crack plane in glass; presumably this angle is dictated by material properties in the sense that the angle is governed by the maximum allowable mode mix that can exist without fragmentation.

At the other extreme of pure mode III loading Knauss (1970) showed that the crack front immediately fragments into multiple cracks, with each facet oriented at an angle of 45° with respect to the original fracture plane (see Fig. 2b); these experiments were performed in a Solithane elastomer that exhibits brittle fracture, behaving more like a rubber, but failing at smaller strain levels. Knauss concluded that these were opening mode cracks, generated perpendicular to the major principal axis. There appears to be some misconceptions in the literature regarding the geometry and emergence of these multiple crack segments. From our experimental observations we recognize that these cracks nucleate along the crack front at a spacing dictated by elastic field interactions between the different nuclei, but modulated by statistical variations in the material properties and fluctuations in the crack front geometry. The geometry of growth of these cracks is such that they develop ahead of the crack as well as behind as they intersect with the top and bottom surfaces of the original crack (see illustration in Fig. 2c).

Cooke and Pollard (1996) performed experiments to examine combined modes I + III; they used a special fixture to augment a typical compact tension specimen with a transverse loading that provided a combined shear loading. They observed that the crack propagated along a helicoidal surface and suggested that this surface is developed by a continuous twisting of a crack front about an axis along the direction of crack extension. We note that the loading in this specimen corresponds to a combination of modes I, II + III, with the mode II component dominating the mode III contribution near the free surfaces of the specimen; the presence of mode II has a major role in dictating the crack surface evolution. Cooke and Pollard (1996) determine the orientation simply by determining the principal direction corresponding to the plane-strain mode I crack tip state under a superposed mode III; this yields

$$\left(\frac{1}{2}-\nu\right)\tan 2\phi = \frac{K_{\mathrm{III}}^{\infty}}{K_{\mathrm{I}}^{\infty}} \tag{1}$$

Observations in the literature, such as those of Yates and Miller (1989) also support a correlation between the twist angle and the ratio of stress intensity factors based on the idea of a locally opening mode crack. Cooke and Pollard (1996) also use the maximum energy release rate criterion, the requirement that mode III on incipient crack equal to zero ($K_{\mathrm{III}} = 0$), and the condition that mode I on the incipient crack K_{I} is a maximum and show that all four criteria predict the same twist angle as a function of $K_{\mathrm{III}}^{\infty}/K_{\mathrm{I}}^{\infty}$ as long as $K_{\mathrm{III}}^{\infty}/K_{\mathrm{I}}^{\infty} < 1.4$; beyond this level the maximum energy release rate criterion exhibits two solution branches. Their experimental results indicate a large divergence from the twist angles predicted by these criteria. They suggest that the interaction between the growing segments might contribute to this discrepancy. While this is definitely a big influence as the crack begins to grow, at initiation, we suggest that the deviations between experiments and predictions may be more due to the fact that the ratio $K_{\mathrm{III}}^{\infty}/K_{\mathrm{I}}^{\infty}$ is calculated based on nominal geometry and two-dimensional analysis, where as the actual state in the specimen is clearly three-dimensional with $K_{\mathrm{III}}^{\infty}/K_{\mathrm{I}}^{\infty}$ varying along the crack front and influenced significantly by the local fluctuations in the geometry. Furthermore, one cannot rule out the influence of mode II as we demonstrate in Sect. 4.

Hull (1993, 1995) examined the problem of mixed mode I + III in great detail and provides an excellent geometrical description of the evolution of the crack

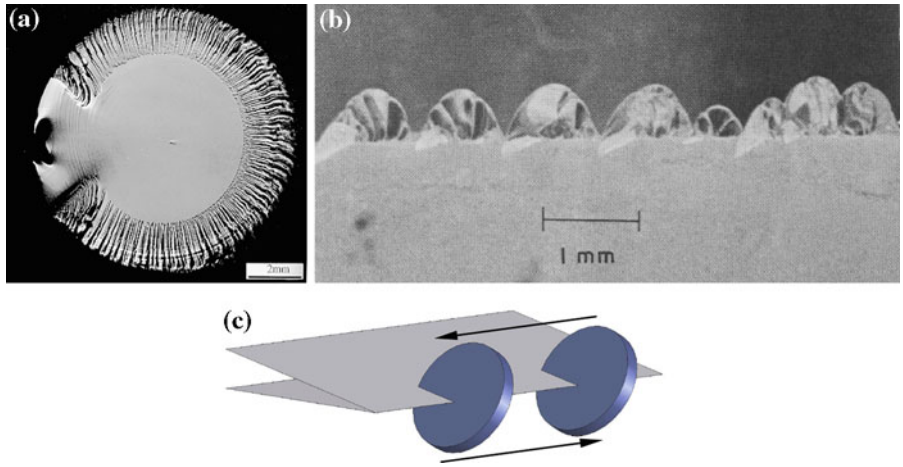

Fig. 2 **a** Fragmentation of the crack front in a glass rod subjected to mode I + III observed by Sommer (1969); **b** Fragmentation of the crack front in a solithane specimen subjected to pure mode III loading (from Knauss 1970); **c** Illustration of the geometry of the nucleation of cracks under superposed mode III loading. The *arrows* indicate the sense of mode III loading

surface; in particular, he discriminates between two possible modes of crack surface evolution. First, Hull (1993) suggests that smooth surfaces with continuous variation of surface normal arise by a successive tilting of the crack, *without any twisting*. He demonstrates this idea by applying it to the helicoidal surface observed later by Cooke and Pollard (1996). In this model, if one abandons the idea that the crack front is straight, then the helicoidal surface can be generated by a continuous tilt variation along the crack front, without any twisting. *Hull's main hypothesis is that smooth crack surfaces do not evolve by twisting, but simply by turning according to the directions dictated by the principal curvatures*. The second mode is related to discontinuous surface evolution; sudden rotations of the principal directions by the imposition of a mode III require a twist of the crack surface about the crack extension direction, and this can only be accommodated by fragmentation of the crack surface as in the observations of Sommer (1969) and Knauss (1970). Once new crack segments are nucleated, they alter the local stress state and further evolution of the individual fragment surfaces evolve continuously unless again forced to fragment further by the external stress state.

There are numerous analytical and numerical investigations of the problem of mixed mode I + III fracture. They may be classified under two categories: in the first category are investigations that aim to determine the stress intensity factors $[K_{\mathrm{I}}, K_{\mathrm{II}}, K_{\mathrm{III}}]$ corresponding to specific boundary value problems; these results are of interest when one characterizes the critical state at fracture. For example, the Handbook of Stress Intensity Factors (Murakami 1987) contains stress intensity factor calculations for various geometrical and loading conditions. Such solutions are useful in characterizing the fracture toughness of materials under combined mode loading; this is illustrated in the works of Schroth et al. (1987) and Davenport and Smith (1993), among others, who determine critical values of $\left[K_{\mathrm{I}}^{c}, 0, K_{\mathrm{III}}^{c}\right]$ at which crack initiation occurs, independently of the development of the fracture surface and path. Such characterization is valuable in providing combined mode crack initiation criterion for use in engineering applications, but does not provide any insight into the growth of cracks and the evolution of the crack surface. In the second category are studies aimed at determining the stress intensity factors $[K_{\mathrm{I}}, K_{\mathrm{II}}, K_{\mathrm{III}}]$ at the tip of a perturbed crack, loaded initially by a combination of $\left[K_{\mathrm{I}}^{\infty}, K_{\mathrm{II}}^{\infty}, K_{\mathrm{III}}^{\infty}\right]$; these solutions are generated in order to determine the criterion (or criteria) for crack path selection and thereby enable simulation of tortuous crack surface evolution Under arbitrary mixed mode loading. The works of Gao and Rice (1986), Gao (1992), Amestoy and Leblond (1992), Xu et al. (1994), Movchan et al. (1998), Lazarus and Leblond (2001a,b), and others represent the major works in this area. The thrusts of these papers range from a simple calculation of the stress intensity factors in the perturbed state, to the evaluation of the stability of such cracks in order to make contact with experimental observations. We remark that the recent work of Lazarus and Leblond (2001b) is a major attempt to extract appropriate failure criteria from comparison to experiments. We discuss the results of Xu et al. (1994) and Movchan et al. (1998) in order to provide context for the present work.

The applied far field loading on the crack is assumed to be dominant mode I, zero mode II and a small superposed mode III component: $[K_{\mathrm{I}}^{\infty}, K_{\mathrm{II}}^{\infty} = 0, K_{\mathrm{III}}^{\infty} \ll K_{\mathrm{I}}^{\infty}]$. In a typical fracture problem, we seek to determine the tilt and twist angles of the crack path by enforcing an appropriate fracture criterion; it is possible to impose different fracture criteria in order to determine the crack response to mixed-mode loading. Let us consider two options: first, that mode II is zero along the perturbed crack along with the energy criterion governing the initiation of the crack; these are written as

$$K_{\mathrm{II}}(s) = 0 \tag{2}$$

$$K_{\mathrm{I}}^2(s) + \frac{1}{1-\nu} K_{\mathrm{III}}^2(s) = EG_c(K_{\mathrm{III}}/K_{\mathrm{I}}) \tag{3}$$

where $G_c(K_{\mathrm{III}}/K_{\mathrm{I}})$ is possibly a function of the ratio of the local mode-I, mode-III combination and where E is the Young's modulus. We will refer to this as Criterion 1. The second option considered is motivated by experimental observations of facet formation. In this instance, we should take the local mode I symmetry condition to dictate that at the perturbed crack tip the only nonzero component of stress intensity factor is the mode I component; we will refer to this as Criterion 2:

$$K_{\mathrm{I}}(s) = K_{IC}, \quad K_{\mathrm{II}}(s) = 0, \quad K_{\mathrm{III}}(s) = 0 \tag{4}$$

$K_{IC} = \sqrt{EG_c(0)}$ is the fracture toughness expressed in terms of the stress intensity factor. Both criteria are a consequence of the principle of local symmetry originally developed by Goldstein and Salganik (1974) for arbitrary three-dimensional crack problems.

There does not appear to be a completely satisfactory estimate of the stress intensity factors along a perturbed crack tip that can be used to evaluate the consequences of the above criteria. Xu et al. (1994) point to errors in the analysis of Gao (1992), while Movchan et al. (1998) find that the analysis of Xu et al. (1994) contains some errors. Lazarus and Leblond (2001a) comment that all the previous authors have perturbed the entire crack front and not just the extension of the crack; their calculations of the stress intensity factors, however, depend on the ratio of crack extension to the segment width and are therefore difficult to apply to the problem of initiation. Xu et al. (1994) considered a problem in which a linearly decreasing perturbation was imposed only over a distance a from the crack tip. Consider a flat, semi-infinite crack which lies in the $x_2 - x_3$ coordinate plane with a straight crack front along $x_2 = 0$. This crack front is first perturbed in the plane of the nominal crack (providing a wavy crack front) such that

$$\delta a(s) = a + B \sin ks + C \cos ks \tag{5}$$

where s is the position along the crack front in the unperturbed crack and δa is the extent of perturbation in the fracture plane. It is then perturbed out-of-plane with respect to the nominal crack surface such that

$$\delta h(x_2, x_3) = \begin{cases} (a + x_2)(\gamma + \omega \sin kx_3) & x_2 > -a \\ 0 & x_2 \le -a \end{cases} \tag{6}$$

where δh is the magnitude of the out-of-plane perturbation. We consider this to be more appropriate than a uniform sinusoidal perturbation over the entire crack surface. The applied far field loading of the unperturbed crack is dominant mode I, zero mode II and a small superposed mode III component, $\left[K_{\mathrm{I}}^{\infty}, K_{\mathrm{II}}^{\infty} = 0, K_{\mathrm{III}}^{\infty} \ll K_{\mathrm{I}}^{\infty}\right]$; however, in light of the errors in the weight functions that are pointed out by Movchan et al. (1998), we take the simpler form of perturbation where the analysis of Xu et al. (1994) and Movchan et al. (1998) appear to agree at least in form, if not in the detailed constants. This corresponds to a perturbation of the crack surface $x_2 < 0$ of the form:

$$\delta h(x_2, x_3) = \varepsilon \sin kx_3 \tag{7}$$

The stress intensity factors at the perturbed crack are given by (neglecting the T-stress terms)

$$\begin{bmatrix} K_{\mathrm{I}}(x_3) \\ K_{\mathrm{II}}(x_3) \\ K_{\mathrm{III}}(x_3) \end{bmatrix} = \begin{bmatrix} 1 + \varepsilon k \left\{ \frac{1}{2} - \frac{1-2\nu}{\sqrt{2}} \right\} \sin kx_3 & \varepsilon k \left\{ 2 - \frac{1-2\nu}{\sqrt{2}(1-\nu)} \right\} \cos kx_3 \\ \varepsilon k \frac{2-3\nu}{2(2-\nu)} \sin kx_3 & 0 \\ 2\varepsilon k \frac{1-\nu^2}{(2-\nu)} \cos kx_3 & 1 \end{bmatrix} \begin{bmatrix} K_{\mathrm{I}}^{\infty} \\ K_{\mathrm{III}}^{\infty} \end{bmatrix} \tag{8}$$

The expressions given by Xu et al. (1994) differ from the above only in the coefficients multiplying the sine and cosine terms.

Applying Criterion 1, we get

$$[K_{\mathrm{I}}^{\infty}]^2 + \frac{1}{1-\nu}[K_{\mathrm{III}}^{\infty}]^2 + 2\varepsilon A k^2 K_{\mathrm{I}}^{\infty} K_{\mathrm{III}}^{\infty} \left[2 - \frac{1-2\nu}{\sqrt{2}} + 2\frac{1-\nu^2}{2-\nu} \right] \sin kx_3 = EG_c \left(K_{\mathrm{III}}^{\infty} / K_{\mathrm{I}}^{\infty} \right) \tag{9}$$

It is clear from that above that the sinusoidal perturbation is not admissible from the point of view of

the energy criterion. Applying Criterion 2, we find once again that the sinusoidal perturbation is inadmissible. Extending these conclusions to the more appropriate form of perturbation described in Eqs. (5) and (6) requires significant additional effort. However, if the tapering of the perturbations along the negative x_2-direction is small, the results of the uniform perturbation discussed above might still hold. Based on this, we surmise that such sinusoidal perturbations cannot be sustained and that the crack front must break up into distinct fragments.

Lazarus and Leblond (2001a,b) performed a detailed analysis of the stress intensity factors for cracks loaded under arbitrary $\left[K_{\mathrm{I}}^{\infty}, K_{\mathrm{II}}^{\infty}, K_{\mathrm{III}}^{\infty}\right]$ with the crack front perturbed locally; their main focus was on the determination of the stress intensity factors, energy release rates and their implication primarily on the rate of rotation of crack planes as the crack front extended; comparison of their predictions to experimental observations on the rate of rotation were found to be satisfactory. In more recent work Lazarus et al. (2008) used finite element analysis to calculate the stress intensity factors and compare the rate of rotation of the crack front with four-point bend experiments and found better correlation. However, neither work addresses the problem of spacing of the crack front fragmentation. In fact, in their concluding paragraph, Lazarus and Leblond (2001b) provide some conjectures on possible failure criteria for crack front fragmentation; in particular, they suggest that the scale of fragmentation of the crack front might depend on a competition between tensile fractures and shear in complementary zones. This is the primary focus of our investigation; we impose the criterion that the crack is under locally opening mode with both $K_{\mathrm{II}} = 0$ and $K_{\mathrm{III}} = 0$ and then based on experimental observations, we propose a new criterion for crack front fragmentation.

3 A criterion for crack front fragmentation

In contrast to the fracture criteria discussed above, we postulate a simple criterion motivated by the following physical observations about the segmentation of the crack front. First, it is evident from experimental observations that, except possibly in the case of extremely small ratios,[1] of $K_{\mathrm{III}}^{\infty}/K_{\mathrm{I}}^{\infty}$ the crack surface 'reorients' itself perpendicular to the direction of maximum tension when propagation ensues under mixed mode I + III and such crack surface reorientation is accompanied by a segmentation or fragmentation of the crack front itself into multiple new crack fronts. So, we will impose that both $K_{\mathrm{II}} = 0$ and $K_{\mathrm{III}} = 0$ on the incipient crack and allow such fragmentation to occur; this was the main reason Criterion 2 was examined in Sect. 2 with respect to smooth (continuous) crack surface perturbations. As a result of such rotation and crack front fragmentation, the cross-section perpendicular to the crack surface exhibits a profile that is sometimes called the "factory roof" profile; this geometry is illustrated in Fig. 3. Let us denote the angle that the fracture plane makes with respect to the original crack surface by ϕ, the spacing between two such fragments by b, and the projection of the segmented crack on to the nominal initial crack plane by d. Lazarus and Leblond (2001a,b) distinguish between two types of cracks corresponding to the two twist angles in the factory-roof pattern. Cracks of type A, indicated in red in Fig. 3a, are formed by opening mode loading and are typically called *en echelon* cracks in the geological and rock mechanics literature (Pollard et al. 1982). Cracks of type B are indicated by the black dotted line in Fig. 3a; it is easily shown that such cracks are not allowable by the maximum normal stress criterion; Lazarus and Leblond (2001a,b) demonstrate carefully that the energy release rate criterion favors type A cracks over type B. Therefore, the type B cracks cannot form concurrently with the type A cracks. Nevertheless, in order for the rupture to propagate, the type A cracks must somehow be connected to each other, expending greater energy[2] than the type A cracks; we suggest that fracture or separation along type B cracks occurs at a later stage in the crack growth than the development of type A cracks and the manner in which the type A cracks link is not necessarily by the formation of the type B cracks shown in Fig. 3a.

The generation and linking of the type A cracks was first explored through dynamic crack growth experiments. A schematic diagram of the growth of a crack under mixed modes I + II + III loading is shown in Fig. 4a. In this experiment, a planar crack located in

[1] The case of small $K_{\mathrm{III}}^{\infty}/K_{\mathrm{I}}^{\infty}$ will be considered briefly in Sect. 5.

[2] Since type B cracks are not favorably oriented with respect to local mode I loading, other more dissipative mechanisms must intervene in order to generate these cracks; this dissipation may involve plasticity, friction or other mechanisms and hence type B cracks are expected to require more energy.

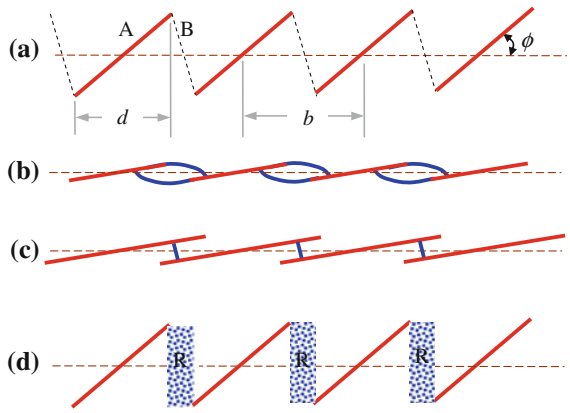

Fig. 3 **a** Geometry of the "factory roof" profile in a plane perpendicular to the crack propagation direction; the *red lines* indicate type A cracks inclined at an angle ϕ with respect to the nominal crack plane and the *black dashed lines* indicate type B cracks; **b** "Hand-shaking" mode of linking of the type A cracks; **c** Bridging cracks linking type A cracks formed after rearrangement of the stress field; **d** Representation of bringing regions R that connect the type A cracks and provide energy penalty for the overall extension of the crack

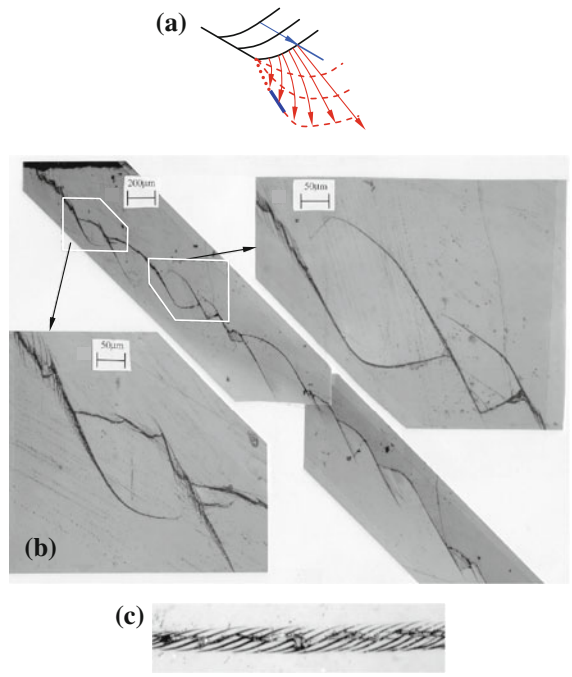

Fig. 4 **a** Geometry of kinking and twisting of a planar dynamic crack subjected to mixed-mode loading; **b** Profile of the crack front in a plane perpendicular to the nominal propagation direction of the crack; **c** Fine scale echelon cracks in PMMA

the interior of a Homalite-100 specimen is subjected to a large shear loading by the arrival of a stress wave; in response to this sudden loading dominated by the mode II, the average plane of the crack twists and grows at an angle γ to the original crack direction, along the path shown by the red arrows in Fig. 4a. While the dominant loading in the interior of the specimen is mode I + II, a portion of the crack is subjected to increasing mode III loading. This mode III contribution results in a fragmentation of the crack. We observe such fragmentation in the cross-section perpendicular to the crack surface when the crack breaks through a free surface in the specimen, highlighted by the blue line in Fig. 4a. Micrographs of the mixed mode I + III crack penetrating a free surface are shown in Fig. 4b, c. As can be seen from the images in Fig. 4, there are multiple levels of crack front fragmentation. It should be noted that unlike the typical "factory roof" pattern, the type B slant cracks that connect the twisted cracks are not always fully developed; in some cases, a smooth curved crack can be observed to link adjacent type A cracks as illustrated schematically in Fig. 3b. In other cases, the gap between the echelon cracks is bridged by opening mode cracks as shown in Fig. 3c that could only have developed significantly later. In some cases, the type B cracks do not form at all, indicating that the surfaces are not fully separated as indicated in Fig. 4b. Based on such observations, we propose that the type A cracks form first, but the region indicated by the shading in Fig. 3d (we will refer to this region as the bridging region) is either uncracked or breaks later; in either case, an energy penalty associated with such regions must be paid as the type A cracks develop. So, we will simply impose the criterion of $K_{\mathrm{III}} = 0$ to determine the twist angle ϕ at any point along the crack front; if this criterion is taken to settle the orientation, then the question of what sets the scale for the length d arises naturally. Two different estimates may be made: one based on steady growth of fragmented cracks maintaining the twist angle and spacing and the other that applies only to initiation of crack growth. However, steady-state conditions are difficult to establish for cracks growing under mixed modes I + III; so we will focus attention on fragmentation of the crack front at initiation of crack growth.

We consider that there is an energy penalty of Γ per unit area for the type A cracks (determined from mode I test results) and a significantly larger energy penalty γ_s per unit volume associated with the bridging regions. The latter energy penalty has to be paid regardless of whether the bridging regions break or simply

deform to accommodate the continued growth of the type A cracks. Then, the local energy dissipation per unit crack extension is equated to the global dissipation as follows:

$$\Gamma d \sec\phi + \gamma_s \alpha d \tan\phi = \tilde{\Gamma}\left(K_{\mathrm{III}}^{\infty}/K_{\mathrm{I}}^{\infty}\right) b \tag{10}$$

where b, d, and ϕ are defined in Fig. 3. The first term on the left hand side of Eq. (10) represents the energy dissipation in the type A slant crack while the second term is the energy dissipated/penalty associated with the bridging region. Note that we take this to be independent of the distance between nuclei assuming non-interacting cracks; also α is taken to be the characteristic width associated with the bridging zone. On the right hand side of Eq. (10), $\tilde{\Gamma}$ is the global fracture energy corresponding to the appropriate ratio of $K_{\mathrm{III}}^{\infty}/K_{\mathrm{I}}^{\infty}$ experienced at the crack tip and can be expressed as:

$$\frac{\tilde{\Gamma}}{\Gamma} = 1 + \frac{1}{1-\nu}\left(\frac{K_{\mathrm{III}}^{\infty}}{K_{\mathrm{I}}^{\infty}}\right)^2 = 1 + \frac{(1-2\nu)^2}{4(1-\nu)}\tan^2 2\phi \tag{11}$$

Note that the angle ϕ is related to the mode mix through Eq. (1). For small crack twist angles, the second term in the right hand side of Eq. (11) is small and may be neglected. Equation (11) is the appropriate fracture criterion to be used in determining the onset of mixed-mode crack growth; that is, we insist that the energy release rate per unit width be adequate to create the new type A cracks and the deformation/dissipation associated with the type B regions. This is a very simple expression of the fact that for a given angle ϕ (or equivalently, the ratio of mode III to mode I loading) the energy penalty in the bridging region increases with d. Note that the maximum allowable value for ϕ is 45° corresponding to a pure mode III loading. Furthermore, note that in the limit of $\phi \to 0, \Gamma d \to \tilde{\Gamma} b$, corresponding to pure mode I loading. Equation (10) can be expressed in normalized form in order to provide an expression for the determination of the fragmentation spacing:

$$\bar{d} = \left[1 + \frac{(1-2\nu)^2}{4(1-\nu)}\tan^2 2\phi\right](\sec\phi + \bar{\gamma}_s \tan\phi)^{-1} \tag{12}$$

where $\bar{d} = d/b$ and $\bar{\gamma}_s = \gamma_s \alpha/\Gamma$. Equation (12) is the relationship between the twist angle and the fragment spacing, and is the required fracture criterion that is to be added to Criterion 2. The main remaining concern relates to how the energy penalty of the type B regions and the scale of nonlocality in Eq. (12), b, can be determined. Analytical estimates of these quantities would require a 3D solution of the fragmented crack front with just the type A cracks, perhaps incorporating nonlinear material behavior in the bridging regions; this is a rather difficult problem. We show in the following sections that when experimental observations of crack spacing are properly interpreted, all these fracture parameters may be extracted.

4 3D variation of stress intensity factors along the crack front

In practical terms, pure mode III is possible only in the case of torsion of a cylindrical bar with either an interior or exterior crack; while this was the configuration used by Sommer (1969), he focused his attention on a dominant mode I loading and a small perturbing mode III. The large plate configuration used by Knauss (1970) approaches nearly pure mode III conditions over the central segment of the crack line; this is the region in which he observed multiple crack nucleation at an angle to the main crack. The bending configuration used by Hull (1993) and others cannot result in a pure mode III or even a combination of modes I + III; this is also true of the compact tension specimen used by Cooke and Pollard (1996). One can argue (and show quantitatively) that a mode II component of singularity must also exist in the vicinity of the free surface. Therefore, in most experiments that were performed to examine mixed modes I + III fracture, the effect of a combined mode II was *always* present, but neglected by the investigators. Furthermore, many of the experimental schemes have not been analyzed completely with a 3D elastic analysis and investigators have relied on ad hoc estimates of the crack tip state. In the present study, a three-point bending configuration was used with asymmetrically oriented cracks to generate mixed-mode loading; this geometry is illustrated in Fig. 5a. A symmetric Galerkin boundary element program (Li and Mear 1998; Li et al. 1998) was used to compute the stress intensity factors, $\left[K_{\mathrm{I}}^{\infty}, K_{\mathrm{II}}^{\infty}, K_{\mathrm{III}}^{\infty}\right]$ for the three-point bending specimens. Some representative results are shown in Fig. 5. It is important to bear in mind the following characteristics of the stress intensity factor variation while interpreting the experimental results from this specimen configuration.

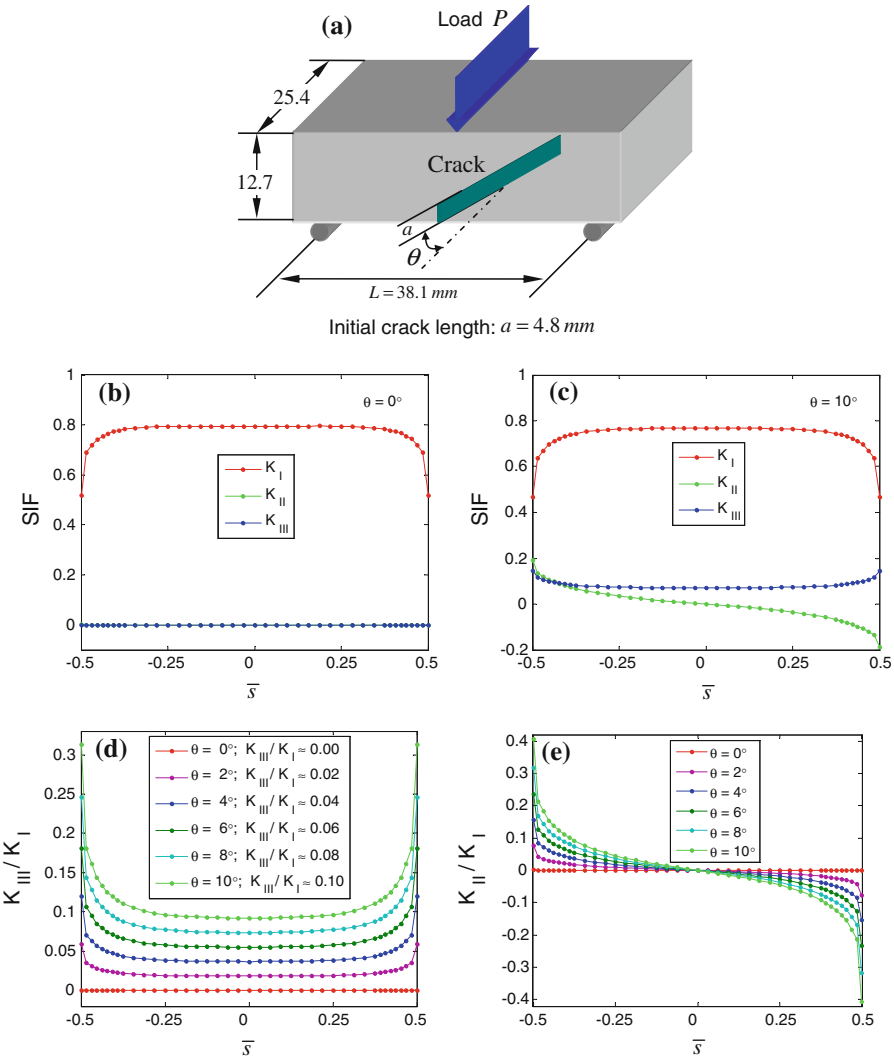

Fig. 5 Stress intensity factor variation for the asymmetric bending configuration. The mode-mixity is controlled by changing the orientation θ of the initial crack. The geometry of the three-point bending specimen is shown in (**a**). The stress intensity factor variation across the specimen width for a specimen with $\theta = 0°$ (pure mode I) and $\theta = 10°$ are shown in (**b**) and (**c**), respectively. The mode mix ratios $K_{\mathrm{III}}^{\infty}/K_{\mathrm{I}}^{\infty}$ and $K_{\mathrm{II}}^{\infty}/K_{\mathrm{I}}^{\infty}$ across the specimen width for different crack orientations are shown in (**d**) and (**e**), respectively

– For the case of the pure mode I specimen, corresponding to $\theta = 0°$, three dimensional effects are observed in the stress intensity factor variation along the crack front (see Fig. 5b; we denote the normalized length along the crack as $\bar{s} = s\cos\theta/h$). It is evident that the mode I stress intensity factor is uniform along the crack front for $|\bar{s}| < 0.35$ and that there is a dramatic drop in K_{I} near the face layers. This is quite well-known (see for example, Raju and Newman 1977 and Sukumar et al. 2000) and results in a thumb-nail shaped crack front in such thick specimens.
– For the case of $\theta = 10°$, three dimensional variation of K_{I} across the specimen width persists as indicated above. In addition, a non-zero mode III contribution (blue line) is observed (see Fig. 5c); this is the combination of modes I + III that we desire in this investigation. While it is tempting to interpret the results from this geometry in terms of simple mode I + III loading, it is clear from the results displayed that this would be erroneous!
– An anti-symmetric variation of the mode II stress intensity factor is seen across the width of the specimen in Fig. 5c; this is non-negligible in comparison to the mode III stress intensity factor for different angles as shown in Fig. 5d and e. In particular, as $\bar{s} \to \pm 0.5$, K_{II} is greater than K_{III} indicating that near the free surfaces of the specimen, the effect of mode II loading will overwhelm the mode III effect. We note that the

helicoidal shape of the crack surface observed by Cooke and Pollard (1996) is most likely due to a mode II component in their specimen that is analogous to the one considered here; the crack deflection observed in their experiments is consistent with what one would expect under combined modes I + II + III.

– Indeed, for all the crack angles $\theta > 0$ examined, there is no part along the crack front (except the point at $\bar{s} = 0$) where the mode II stress intensity factor is zero. Therefore, one must be extremely careful in interpreting experimental observations in terms of the mixed-mode loading.

In order to interpret the results of our experiments in terms of combined modes I + III, we will restrict our attention to $|\bar{s}| < 0.012$; within this range, the ratio of $K_{\mathrm{II}}/K_{\mathrm{I}}$ is always less than about 0–0.02 while $K_{\mathrm{III}}/K_{\mathrm{I}}$ is in the range of 0–0.15 (see Fig. 5). This restriction was made to ensure a dominant combined mode I + III loading in the specimens.

5 Experimental results and interpretation

Three-point-bend tests were performed on numerous specimens, with the crack oriented at angles $\theta = [2, 4, 6, 8, 10]°$. Both the global response (defined by the load vs load-point displacement) and the local response (characterized by qualitative and quantitative microscopy) were determined. These are discussed in this section.

5.1 Global response under mixed-mode loading

Three point bend experiments were performed on Homalite-100 specimens. The nominal specimen dimensions are shown in Fig. 5; the specimens were machined to high geometrical tolerance. The crack was cut with a diamond saw and then sharpened by scribing with a razor blade. This results in a macroscopically straight, sharp crack front. The load vs load-point displacement variation for the three-point bend test in Homalite-100 were monitored during the tests; these specimens behaved linearly until the onset of unstable crack growth, with the crack popping across the entire specimen dynamically at onset of failure; no

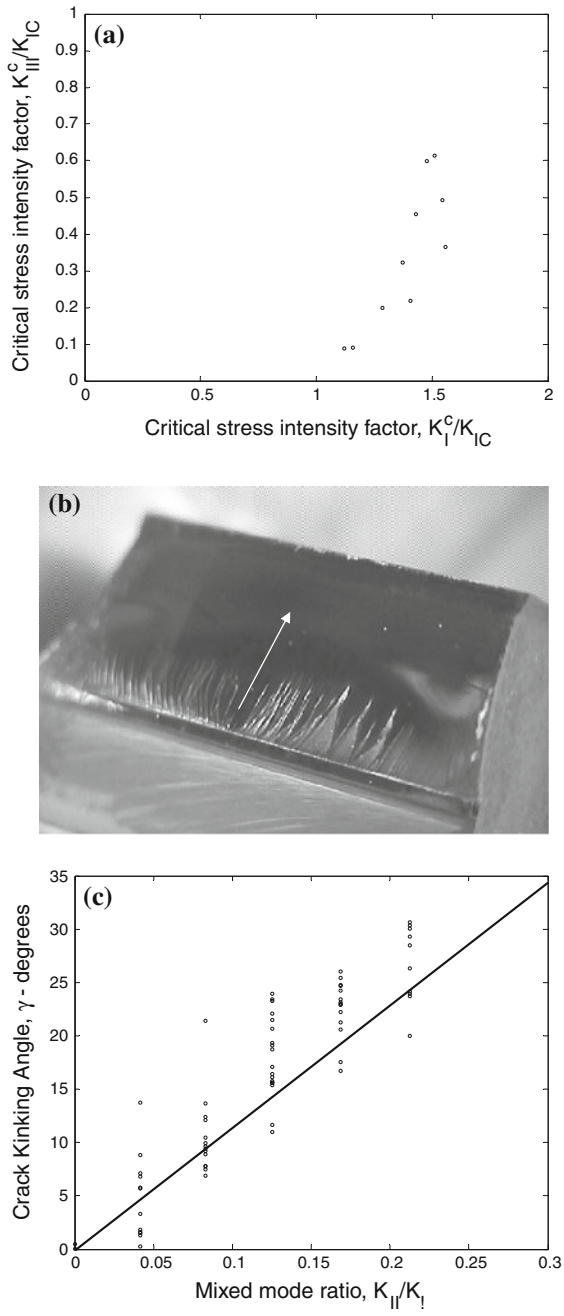

Fig. 6 **a** Critical stress intensity factors for crack initiation under mixed modes I + III in Homalite 100. **b** Photograph of fracture surface showing the helicoidal surface as well as the fine scale roughness in the first few mm of crack extension; direction of crack extension is indicated by the *arrow*. The kink angle at the free surface of the specimen, caused by the mode II component is clearly visible in the photograph. **c** Plot of the tilt angle γ versus the ratio of $K_{\mathrm{II}}/K_{\mathrm{I}}$ corresponding to Homalite 100

measurements were made during the growth phase of this experiment. The nominal values of $\left[K_{\mathrm{I}}^{c}, 0, K_{\mathrm{III}}^{c}\right]$, calculated based on the peak measured load are plotted in Fig. 6a; these correspond to the values of the mode I and mode III stress intensity factors at the midplane of the specimen where the mode II stress intensity factor is zero. Since the crack angle was varied over a small range, the magnitude of mode III stress intensity factor used in these experiments is quite small; if a complete characterization of fragmentation is required, the entire range of $K_{\mathrm{III}}^{\infty}/K_{\mathrm{I}}^{\infty}$ should be investigated. However, our interest is in the characterization of crack front fragmentation and the range used is adequate for this purpose. The "nominal" crack surface develops into a helicoidal shape that Hull (1993), Cooke and Pollard (1996) and others have described; a photograph of the fracture surface is shown in Fig. 6b. In fact, while the crack surface exhibits significant roughness in the early stages, after the crack extends about 5 mm, the surface becomes mirror-like and evolves smoothly apparently obeying the no-twist criterion suggested by Hull (1993). The evolution of the helicoidal surface of the crack is governed by the combination of mixed modes I + II + III. In order to demonstrate this clearly, we examine the crack path where the crack surface meets the free surfaces of the specimen at $\bar{s} = \pm 0.5$; the numerical analysis discussed in Sect. 4 clearly indicates that the ratio of $K_{\mathrm{II}}^{\infty}/K_{\mathrm{I}}^{\infty} \neq 0$, but depends on the crack orientation, θ. The criterion of local symmetry indicates that for small amplitudes of K_{II}^{∞} the crack should kink at an angle $\gamma = -2K_{\mathrm{II}}^{\infty}/K_{\mathrm{I}}^{\infty}$; Fig. 6c shows the experimentally measured kink angle γ on the free surfaces of the specimen as a function of the corresponding mode I + II loading ratio, $K_{\mathrm{II}}^{\infty}/K_{\mathrm{I}}^{\infty}$ evaluated at $\bar{s} \sim 0.5$. It is clear from this result that the mode II loading is a crucial factor in driving the helociodal surface of the specimen. If the mode II component is absent, as is the case towards the midplane of the specimen, the role of mode III loading is to lead to fragmentation of the crack front. The exception to this occurs in the case of very small mode III perturbations discussed by Bonamy and Ravi-Chandar (2003, 2005); we discuss this briefly at the end of this section.

In order to determine the appropriate crack front fragmentation criterion, the global measurements discussed above do not provide any guidance; one must focus on the region close to the initial crack tip and furthermore near the middle of the specimen where nearly pure mode I + III loading condition exits and examine the local response in this region.

5.2 Characterization of the local response under mixed-mode loading

A magnified view of the fracture surface in the region $|\bar{s}| < 0.012$ is shown in Fig. 7a; the initial crack surface and crack front are marked in this figure. Clearly, the crack front fragments immediately at crack initiation. We will attempt to extract the appropriate fracture criterion from local measurements of the geometric features of the fracture surface. One of the main hurdles in interpreting experimental results found in the literature concerning failure criterion is that most investigators have simply used the calculated "nominal" stress intensity factors to be the actual stress intensity factors and attempted to interpret the twist angles and segmentation. For example, Lazarus and Leblond (2001b) show that there are significant deviations between the analytical predictions and experimental observations of the evolution of the fracture surface geometry. However, we note that in interpreting experiments we must account for the fact that the actual crack was introduced by cutting with a diamond saw with the tip sharpened by scribing with a sharp razor blade. This is far from the idealized crack surface and crack front assumed in the analyses, and obviously these deviations from the ideal will manifest themselves on the progression of the mixed-mode fracture at the microscale where the crack front and surface are observed. Therefore, in interpreting the experimental observations, it is important to take into account not only the thickness dependence of the stress intensity factors discussed above in Sect. 4, but also to keep in mind that the "local" value of the stress intensity factors along the crack front will be perturbed from the calculated values due to the deviations from the ideal geometry of both the crack surface and the crack front. Since these perturbations are not easily characterized, we simply note that these perturbations as well as local fluctuations in the fracture toughness of the material, will appear as fluctuations in the experimentally observable quantities: the fracture twist angle and the crack fragment spacing.

Quantitative evaluation of the twist angle ϕ from the fracture surfaces was obtained by interference microscopy with a WYCO RST Plus Optical Profilometer.

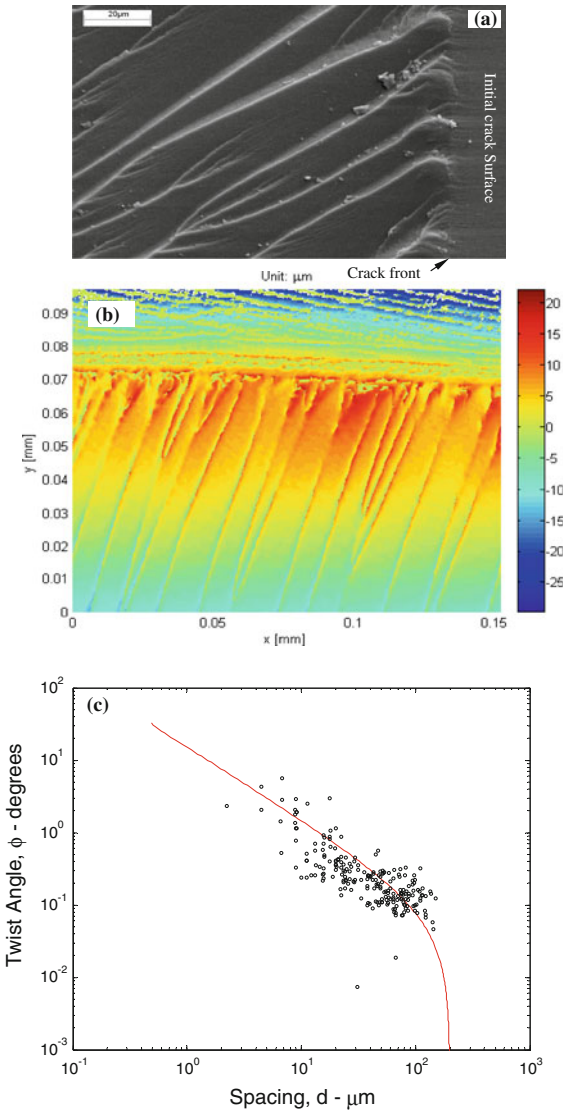

Fig. 7 **a** A typical scanning electron microscopic image of the fracture surface under mixed modes I + III; **b** Profile of the fracture surface obtained with the WYKO Optical Profilometer. Color bar indicates height in microns. **c** Plot of the twist angle ϕ versus the spacing d of the crack fragments corresponding to Homalite 100, with $\theta = 4, 6, 8°$. The red line represents the fitting of Eq. (18) to the data set, with parameters selected by a best fit criterion

In the image shown in Fig. 7b, the field of view is about $150\mu\text{m} \times 100\mu\text{m}$; the color bar in the legend indicates height above a nominal reference plane in μm. One can infer from this image that the twist angles ϕ of the fragmented cracks surfaces are not all equal, even though the global loading indicates a constant value of $K_{\text{III}}^{\infty}/K_{\text{I}}^{\infty}$ and hence that a constant value of ϕ should be established in the central region of the specimen. We will consider the relationship between ϕ and $K_{\text{III}}^{\infty}/K_{\text{I}}^{\infty}$ to be given by the opening mode criterion in Eq. (1) and propose that variations in the twist angle ϕ are due to the statistical variability in the local geometry that results in variations of $K_{\text{III}}/K_{\text{I}}$. It is also apparent from Fig. 7b that the spacing between fragments of the twisted crack surfaces is not uniform, but exhibits significant variations along its path.[3] From a large collection of such measurements, we plot the dependence of the fragment spacing d on the twist angle ϕ in Fig. 7c; some of the variability in these measurements arises from the fact that both ϕ and d change along the direction of crack extension, but the model is expected to apply only at the onset of fragmentation of the crack front. The reasons for expecting a correlation between these two quantities were already discussed in detail in Sect. 3. Fitting the model in Eq. (12) to the experimental results in Fig. 7c, we extract the parameters: $b = 200\,\mu$m which is of the order of the fracture process zone in Homalite-100 and $\bar{\gamma}_s = 750$, suggesting that the energy penalty in bridging regions is much higher than the fracture energy.

Thus, we believe that we have an appropriate fracture criterion under mode III loading: first, the crack picks the direction ϕ along which both $K_{\text{II}} = 0$ and $K_{\text{III}} = 0$; second, the crack front fragments into multiple cracks with the spacing d dictated by Eq. (12) with the material parameters Γ, γ_s, and b determined through calibration experiments. Of course, additional confirmation of this criterion, with other materials and in other geometrical conditions, is required.

It is interesting to speculate how one might use this fracture criterion in simulations of crack growth. Asserting that both $K_{\text{II}} = 0$ and $K_{\text{III}} = 0$ on the prospective crack, first we find the plane through the use of Eq. (1). However, instead of extending the entire crack front, one must select discrete nuclei spaced at a distance dictated by Eq. (12); we can then extend the crack over a small increment according to the energy criterion and then recalculate the local values of the stress intensity factors. At this point, this remains a speculation since we have not addressed the issue of actual computation, evaluation of convergence, and comparison

[3] This is possibly due to the presence of mode II loading as well on the microscale; we have not examined this aspect in the present paper, although this data can be interpreted through the analysis of Lazarus and Leblond (2001a,b).

to experimental measurements; these remain as future tasks.

We have focused on a single issue associated with the mixed-mode I + III loading—the development of fragments at crack initiation. Are there situations where such fragmentation does not occur? The experiments of Bonamy and Ravi-Chandar (2003, 2005) provide some clues concerning this question. In an investigation of crack front waves, they imposed small amplitude local mode III perturbations on propagating mode I cracks in glass specimens. The fast running mode I cracks were generated in wedge-loaded specimens; the cracks typically propagated at speeds in the range from about 400 to about 1,200 m/s. The mode III perturbation was generated by a short duration shear stress pulse generated with a piezoelectric ultrasonic transducer and made to impinge on the running crack tip. This interaction creates a transient perturbation on the mode I crack also spatially localized over the domain of interaction between the ultrasonic pulse and the propagating crack. In response to this perturbation, the crack front undergoes a continuous undulation without the fragmentation observed in the more global perturbation of mode III loading that arises in quasi-static problems. The amplitude of surface undulation was in the range of 100 nm, and the spatial extent less than 200μm. This observation suggests that when the length scale over which the mode III perturbation appears is less than the scale of nonlocality, b, crack front fragmentation cannot be triggered by the loading.

6 Conclusion

The problem of crack growth under mixed mode I + III loading is considered in this paper. It is demonstrated that the effect of superposing a small amount of mode III on a crack subjected to predominantly mode I loading is:

(a) to generate a mode I crack perpendicular to the direction of maximum tension, and
(b) to fragment the crack front into multiple cracks with the spacing dictated by the energy requirements of the bridging areas between the multiple cracks.

Furthermore, through an accumulation of experimental data on specimens of Homalite-100, a strong correlation is shown between the spacing d of crack front fragments and the crack twisting angle ϕ. Such a correlation is motivated on the basis of a simple energy balance argument: in order for the segmented crack fronts to develop, the energy penalty associated with the regions bridging the fragmented cracks must be taken into account. With the aid of this model, we reconcile the experimental measurements of crack front fragmentation and extract the scale of nonlocality and the energy penalty associated with the bridging zone.

Acknowledgments The financial support from the National Science Foundation, through grant number CMS-004914, during the performance of this work is gratefully acknowledged.

References

Amestoy M, Leblond JB (1992) Crack paths in plane situations: II detailed form of the expansion of the stress intensity factors. Int J Solids Struct 29:465–501

Bonamy D, Ravi-Chandar K (2003) Interaction of stress waves with propagating cracks. Phys Rev Lett 91 (Art. No. 235502)

Bonamy D, Ravi-Chandar K (2005) Dynamic crack response to a localized shear pulse perturbation in brittle amorphous materials: on crack surface roughening. Int J Fract 134(2005):1–22

Cooke ML, Pollard DD (1996) Fracture propagation paths under mixed mode loading within rectangular blocks of polymethyl methacrylate. J Geophys Res 101:3387–3400

Davenport JCW, Smith DJ (1993) A study of superimposed fracture modes I, II and III on PMMA. Fatigue Fract Engng Mater Struct 16:1125–1133

Gao H (1992) Three-dimensional slightly nonplanar cracks. J Appl Mech 59:335–343

Gao H, Rice JR (1986) Shear stress intensity factors for a planar crack with slightly curved front. J Appl Mech 53:774

Goldstein RV, Salganik RL (1974) Brittle fracture of solids with arbitrary cracks. Int J Frac 10:507–523

Hodogdon JA, Sethna JP (1993) Derivation of a general 3-dimensional crack-propagation law—A generalization of the principle of local symmetry. Phys Rev B 47:4831–4840

Hull D (1993) Tiltig cracks: the evolution of fracture surface topology in brittle solids. Int J Fract 62:119–138

Hull D (1995) The effect of mixed mode I/III on crack evolution in brittle solids. Int J Fract 70:59–79

Knauss WG (1970) An observation of crack propagation in anti-plane shear. Int J Frac 6:183–187

Lazarus V, Buchholz FG, Fulland M, Wiebesiek J (2008) Comparison of predictions by mode II or mode III criteria on crack front twisting in three or four point bending experiments. Int J Fract 153:141–151

Lazarus V, Leblond JB (2001a) Crack front rotation and segmentation in mixed mode I + III or I + II + III. Part I: calculation of stress intensity factors. J Mech Phys Solids 49:1399–1420

Lazarus V, Leblond JP (2001b) Crack front rotation and segmentation in mixed mode I + III or I + II + III. Part II: comparison with experiments. J Mech Phys Solids 49:1421–1443

Li S, Mear ME (1998) Singularity-reduced integral equations for displacement discontinuities in three-dimensional linear elastic media. Int J Fract 93:87–114

Li S, Mear ME, Xiao L (1998) Symmetric weak-form integral equation method for three dimensional fracture analysis. Comput Methods Appl Mech Engrg 151:435–459

Movchan AB, Gao H, Willis JR (1998) On perturbations of plane cracks. Int J Solids Struct 35:3419–3453

Murakami Y (1987) Stress intensity factors handbook. Pergamon, Oxford

Pollard DD, Segall PE, Delaney PT (1982) Formation and interpretation of dilatant echelon cracks. Geol Soc Am Bull 93:1291–1303

Raju IS, Newman JC (1977) Three-dimensional finite-element analysis of finite-thickness fracture specimens, Technical Report NASA TND-8414, NASA Langley Research Center, Hampton, VA 23665

Schroth JG, Hirth JP, Hoagland RG, Rosenfeld AR (1987) Combined mode-I-mode-III fracture of a high strength low alloy steel. Met Trans 18A:1061–1072

Smekal A (1953) Zum Bruchvogang bei sprodem Stoffrerhalten unter ein und mehrachsiegen Beanspringen. Osterr Ing Arch 7:49–70

Sommer E (1969) Formation of fracture 'lances' in glass. Eng Frac Mech 1:539–546

Sukumar N, Moes N, Moran B, Belytschko T (2000) Extended finite element method for three-dimensional crack modeling. Int J Numer Methods Engrg 48:1549–1570

Xu G, Bower AF, Ortiz M (1994) An analysis of non-planar crack growth under mixed mode loading. Int J Solids Struct 31:2167–2193

Yates JR, Miller KJ (1989) Mixed-mode (I–III) fatigue thresholds in a forging steel. Fatigue Fract Eng Mater and Struct 12:259–270